Neural oscillations across olfactory regions encode odorant information in the teleost olfactory system

Jesús **Olivares**[1*], Patricio **Orio**[1,2*], Viktor **Sadílek**[3], Oliver **Schmachtenberg**[1,4ł] and Andrés **Canales-Johnson**[5,6ł]

[1] Centro Interdisciplinario de Neurociencia de Valparaíso (CINV)
[2] Instituto de Neurociencia, Facultad de Ciencias, Universidad de Valparaíso, Valparaíso, Chile
[3] Department of Biosystems Science and Engineering, ETH Zurich, Basel, Switzerland
[4] Instituto de Biología, Facultad de Ciencias, Universidad de Valparaíso, Valparaíso, Chile
[5] Department of Psychology, University of Cambridge, Cambridge, United Kingdom
[6] Vicerrectoría de Investigación y Posgrado, Universidad Católica del Maule, Talca, Chile

ł These authors share corresponding authorship
* These authors share equal contribution

ł **Corresponding authors:** Dr. Andrés Canales-Johnson (email: afc37@cam.ac.uk), and Dr. Oliver Schmachtenberg (email: oliver.schmachtenberg@uv.cl).

ABSTRACT

Field potential oscillations in the olfactory system of vertebrates and invertebrates are prominent and well-studied, but their functions remain nevertheless enigmatic. Spatial networks are thought to play a role in olfactory discrimination in different species, but their analysis is frequently complicated by behavior, learning and respiration (sniffing). Here, we show that in a sniffing-free model (trout), the relevant feature for discriminating odorant identity is the information conveyed by the oscillatory activity in a spatially distributed network, including the olfactory bulb and the telencephalic regions Vv and Dp. Specifically, information-based methods based on spectral decoding, information sharing, and information redundancy distinguished odorant identity across spatially distant regions while classical spectral analyses did not. Our study demonstrates that olfactory oscillations are carriers of spatially distributed odor information across the teleost olfactory system.

INTRODUCTION

The earliest study of field potential oscillations in the olfactory system was probably performed by Edgar Adrian, who recorded this phenomenon from the olfactory system of decapitated fish[1]. A few years later and in the middle of the second World War, he published a seminal and well-cited study describing oscillatory electrical activity in the olfactory system of anesthetized earth urchins[2]. Since then, oscillations have been demonstrated in olfactory pathways of many species, with remarkable similarities between vertebrates and[3–6]. Nevertheless, the phenomenon remains surprisingly enigmatic, because unequivocal proof of the coding of olfactory information and a role in odorant discrimination by olfactory oscillations remains absent to date. Olfactory oscillations are also a complex phenomenon in terms of their origin and structure: There are at least three types of oscillations involved in the central processing of olfactory signals in vertebrates, which vary by frequency, cause of activation, underlying cellular circuitry, spread across brain areas, and physiological implications. However, local bulbar and top-down inhibitory feedback signaling are broadly accepted as physiological roots of olfactory oscillatory activity[7,8].

In mammals, the recorded signals can be classified according to their frequencies as: Delta rhythm (0 - 4 Hz), theta rhythm (4 - 8 Hz), alpha rhythm (8 - 12 Hz), beta rhythm (12 - 30 Hz) and gamma rhythm (30 - 100 Hz)[9]. Among these, the most studied in the analysis of evoked activity in smell are those belonging to theta, beta and gamma rhythms, due to their potential association with olfactory learning and memory processes[10,11].

Theta rhythms, also known as "respiratory oscillations", due to their association with the respiratory cycles of mammals, are characterized by the activation of specific glomeruli during inhalation activity[9], also showing consistency with theta rhythms of the hippocampus under specific learning conditions[6,11]. Although changes dependent on behaviors such as "sniffing" or sleep-wake states are observed in these[9,12], their role in olfactory processing is not well understood, especially considering that there are animals in which the respiratory system is not directly related to the olfactory system. Such is the case among others in teleost fishes[13], in which theta oscillations related to respiratory activity are absent from the olfactory system, although surprisingly a behavior similar to sniffing has been observed in teleost nostrils[14].

The gamma rhythm is the most studied of the neural oscillations[15]. Although its presence is dominant in the olfactory system in the absence of odorants, it is also observed in response to olfactory stimulation[11], having been associated with local processing of odoriferous stimuli[15]. This rhythm consists of two sub-bands in many species, one of high frequency (gamma 1) and one of low frequency (gamma 2), which are modulated by sensory input with different functional associations and represent the fastest oscillations described in the olfactory system[9,15–17]. These oscillations have not been observed in the immature olfactory bulb of rats[18] and specifically the gamma 2 oscillations are absent in anaesthetized animals[9]. In the LFP of the olfactory bulb of the teleost *Danio rerio* (zebrafish), gamma-type oscillations have been recorded with a frequency of 20 - 30 Hz and an onset a few milliseconds after stimulus application[17,19,20].

Beta rhythms have been recorded from different structures of the olfactory systems of many mammalian species, including mice, rats, cats, rabbits, and moles[11], and it has been demonstrated that these oscillations emerge and are modulated by olfactory tasks such as olfactory learning and sensitization to odors[9,11,15,17]. The main difference observed between gamma and beta oscillations is that the former occurs locally within the olfactory bulb, while the latter require intact bidirectional interconnections between the olfactory regions of the bulb and the telencephalon[11,21]. In addition, beta oscillations have never been observed in the absence of olfactory stimulation and may last much longer than gamma oscillations, which decline rapidly after their onset[9,11].

The popularization of wireless and multiple electrode recording systems mounted on freely moving mammals has allowed the recording and analysis of the different types of olfactory oscillations in a more natural context and within well-defined behavioral assays[7,11,22]. However, the complex signals obtained, and the multiple parameters affecting them, including movement, sniffing, learning, memory, and individual variation, have complicated the analysis and understanding of the physiological functions of olfactory oscillations, in spite of the undeniable advance and sophistication of recording techniques in the last decades.

In fish, the olfactory sense plays important roles in social interactions, mating, migration and feeding, among others[23]. The fact that respiration in teleost fish is not related to smell opens the possibility of recording olfactory system activity as an isolated variable compared to mammals, reducing the confounding factors previously mentioned. Although the teleost olfactory system displays great similarities with that of mammals, there are some differences that must be considered for functional odorant analysis. In the teleost olfactory bulb, mitral cells are indistinguishable from tufted cells and innervate multiple glomeruli at once, which are surrounded by short axon cells and periglomerular cells that are involved in the initial processing of olfactory information[17,24–26]. This, added to the existence of another type of projection neurons with an opposite polarity to the mitral cells (ruffed cells) that synapse with granule neurons, may be evidence of slightly different olfactory coding strategies in teleosts[24,26,27].

In the telencephalon, since the brain formation process of teleost fish (eversion) is different from that of most other vertebrates (evagination), a very different distribution of brain structures compared with mammals is generated as a result[23,24]. Additionally, the structures that are homologous to the neocortex or pallium of most terrestrial vertebrates, lack a six-layer cortex or lamellar structures in teleost fish and, instead, contain areas and nuclei neuroanatomically and functionally analogous to the pallial and subpallial structures of other vertebrates, which includes areas that process olfactory information[24,27–29]. Thus, there is evidence that several pallial and subpallial regions of the teleost telencephalon receive projections from the olfactory bulb and among these, the ventral telencephalon region has characteristics that relate it to mammalian reward systems such as the *septum*, the *nucleus accumbens* and the *substantia innominata*, while functions related to the determination of the identity of odors are attributed to posterior dorsal areas of the teleost telencephalon, since it is the main objective of the secondary olfactory fibers, comparable to the primary olfactory cortex and the piriform cortex of higher vertebrates[23,24,30–36].

Here, we took a conservative approach and simplified the sensory setting to a maximum, eliminating the effects of movement and sniffing by recording from anesthetized teleost fish. To reduce intra- and inter-specimen variation, we repeated identical trials many times within and across the specimens and pooled the data for advanced analysis of putative information contents. Specifically, we recorded olfactory responses reflected by LFP activity in parallel from four sectors of the olfactory system in live anesthetized rainbow trout (*Oncorhynchus mykiss*): Olfactory epithelium, olfactory bulb and the ventral core of the ventral telencephalon (Vv) and its posterior dorsal area (Dp). Our data indicate that primary response parameters such as oscillation power, main frequency, time course and phase were robust and largely indifferent to several olfactory stimuli, but a more nuanced analysis based on connectivity and spectral decoding revealed shared information contents between different recording sites, supporting the notion that olfactory oscillations act as carrier waves transmitting subtle information traces across olfactory brain centers.

MATERIALS AND METHODS

Animals, anesthesia and surgery

Juvenile rainbow trout, *Oncorhynchus mykiss*, were obtained from a local hatchery (Piscicultura Río Blanco, Los Andes, Chile), and kept at 16°C in aquariums with dechlorinated and filtered water in the animal facility of the Faculty of Sciences of the Universidad de Valparaíso, for up to six months, with a light / dark regime of 12:12 hours. The animals were fed daily with fish meal pellets. For the experiments, specimens of undetermined sex and a total length of 20 ± 2 cm were selected. The procedures applied in this study were approved by the Bioethics Committee of the Universidad de Valparaíso and are in accordance with the guidelines of the National Research and Development Agency (ANID) of Chile. Before the experiments, the fish were anesthetized with 10 mg/l MS-222 (ethyl 3-aminobenzoate methanesulfonate) and immobilized with an intramuscular injection of gallamine triethiodide (Flaxedil; 0.03 mg / 100 g body weight), until balance and responsiveness were lost. Immobilized fish were wrapped in moistened tissue and placed in a container of synthetic sponge. The gills were irrigated through an oral tube with a constant flow of cooled aerated water (10°C) containing 10 mg/l of MS-222 (pH 7.4). Before surgery, all dissection material was impregnated with lidocaine hydrochloride (2%), which was also applied directly on the surface of the animal's skin. To gain access to the fish's olfactory organ, the skin and connective tissue covering the entrance to the nostril was removed. To access the brain, the cranial vault was opened under a stereomicroscope with a transverse section through the midline of the head at eye level. Then, two cuts were made perpendicular to the first, and the skull was carefully opened until the brain was exposed. From this point on, the brain was periodically irrigated with artificial cerebrospinal fluid (in mM: 124 NaCl, 2.69 KCl, 1.25 KH_2PO_4, 2.0 $MgSO_4$, 26 $NaHCO_3$, 2.0 $CaCl_2$, 10 glucose, pH 7.4). The vitality of the fish was monitored by checking the blood flow in the vessels of the *tela coroidea* covering the telencephalon.

Odor preparation and stimulation

The water to which the trout were adapted in the animal facility (TW, trout water) was used as negative odor control, and to dilute the odorant mixtures. Four different types of odor stimuli were applied throughout the study: (1) A synthetic mixture of five L-amino acids (AA): Serine, cysteine, aspartate, lysine and alanine; a mixture of four synthetic bile salts (BS): Deoxycholic acid, sodium taurocholate, lithocholic acid and taurolithocholic acid; beta-phenylethyl alcohol (PEA) as single odorant stimulus, and an extract of trout skin (SE). Amino acids represent food odors to fish; bile salts are considered to be social odors and PEA is a compound that is used as a fishing lure and as synthetic odorant in zebrafish studies[26,37,38]. Finally, the extract of trout skin is a natural odorant mixture containing alarm pheromones[26,39–41]. The mixture of bile salts (BS), composed of four compounds (deoxycholic acid, sodium taurocholate, Lithocholic acid and taurolithocholic acid) and the mixture of five amino acids (AA) (Ser, Cys, Asp, Lys and Ala). Skin extract (SE) is a mixture resulting from the homogenization of a complex biological tissue, likely composed of hundreds or thousands of compounds[42].

The amino acids and bile salts were prepared as stock solutions at a concentration of 100 mM and subsequently diluted in TW to the final concentration. Skin extract was prepared from the macerated skin of five juvenile trout in 100 ml of TW, filtered and aliquoted as stock solution. The stock was frozen at -80°C and used throughout the study. All chemicals were purchased from Sigma-Aldrich (Santiago, Chile). Approximately equipotent odor stimuli were defined by diluting BS and SE stocks to concentrations generating the same electroolfactogram amplitude as 100 µM of AA, yielding 700 µM for the BS mixture and a dilution of 1: 500 for the SE stock. For PEA, equipotent values could not be obtained, since responses remained smaller up to concentrations above 1 mM. The olfactory

stimuli were administered automatically using a custom-built computer-controlled picospritzer connected to the gravity-fed open perfusion system constantly irrigating the olfactory organ.

Electrophysiological recordings

We recorded the electroolfactogram (EOG) in parallel with the local field potentials (LFP) in the olfactory bulb (OB) and two telencephalic regions, the ventral nucleus of the ventral telencephalon (Vv) and the dorsal posterior zone of the telencephalon (Dp) (**Figure 1A**). All signals were acquired with WinWCP software version 4.3.8 (John Dempster, University of Strathclyde, UK) and analyzed using Clampfit 10.3. (Molecular Devices). The EOG was recorded from the olfactory rosette with an Ag/AgCl electrode located directly above the central raphe. An identical reference electrode was placed on the skin of the head, and a ground electrode connected to a fin. The EOG signals were amplified with a differential AC amplifier (Warner DP-301, Warner Instruments, USA) and digitized with a PCI-6221 A/D interface (National Instruments, USA) at a sampling rate of 1 kHz. For each recorded brain sector, two tungsten electrodes were used (FHC tungsten microelectrode, tip diameter 3 µm, impedance 11-13 MΩ), one at the recording site and the other as a reference, positioned in the cerebrospinal fluid of the exposed cranial cavity. In the olfactory bulb, the electrodes were positioned within the mitral cell layer, about 150 µm deep with respect to the dorsal surface of the bulb. Given the odotopy of the olfactory bulb, the position of the recording electrode was adjusted depending on the stimulus type, based on an odotopy map reported in (Bazáes et al., 2013). The electrode used to record Vv was positioned in the anterior third of the animal's telencephalon at approximately 500 µm from OB and a depth of 150 µm, entering through the central sulcus between the hemispheres. The electrode recording the telencephalic region Dp was positioned in the posterior third of the telencephalon, at 500 µm distance from the optic tectum (OT) and a depth of 450 µm. All recordings were made in ipsilateral brain structures with respect to the stimulated olfactory organ. Each recording protocol had a duration of 50 seconds, which included the application of the olfactory stimulus or control after the first 10 second with a duration of 1 s. Twenty consecutive trails were performed for each stimulus type. The LFP electrodes were connected to the headstages of an AC amplifier (AM Systems Model 1800), band-pass filtered between 1 and 100 Hz and digitized at 1 kHz.

Signal processing and frequency analysis

Signals were low pass filtered at 50 Hz (3 pole Butterworth filter) and downsampled to 200 Hz. Spectral density was calculated using Welch's method, with segments of 500 samples and an overlap of 350. For each experiment, a frequency spectrum was calculated from the 10 s following each of the stimulus exposures, and the spectra were averaged. Similarly, baseline spectra were calculated for the 10 s prior to stimulus application and averaged. The average of baseline spectra was subtracted from the post-stimulus. Spectrograms were calculated using a continuous wavelet transform (CWT) with the complex Morlet wavelet (σ=5). The CWT is defined as:

$$W(t,s) = \frac{1}{s}\int_{-\infty}^{\infty} f(u)\psi^*\left(\frac{u-t}{s}\right)du$$

Where s is the scale parameter, t the position parameter, $f()$ the signal function, $\psi()$ the wavelet function and the asterisk represents the complex conjugate. The complex Morlet wavelet is defined as:

$$\psi(t) = \left(1 + exp\,(-\sigma^2)\ - 2\,exp\left(-\frac{3}{4}\sigma^2\right)\right)^{-\frac{1}{2}} \pi^{-\frac{1}{4}}\,exp\left(-\frac{1}{2}t^2\right)\left(exp\,(i\sigma t)\ - exp\left(-\frac{1}{2}\sigma^2\right)\right)$$

With central frequency $\sim\sigma$. The scaleogram, analog to the spectrogram, is defined as the square of the amplitude of the CWT:

$$X(t,s) = W(t,s)\big(W(t,s)\big)^*$$

The scale is related to the period (T) and frequency (f) in the following relationship:

$$\frac{1}{f} = T \sim s/\sigma$$

The spectrogram amplitudes were expressed as the z-score by subtracting, at each frequency, the mean of the amplitudes of the baseline spectrogram and dividing by its standard deviation.

Coherence analysis

Coherence C_{XY} between signals X and Y was calculated as:

$$C_{XY} = \frac{|P_X^* P_Y|^2}{(P_X P_X^*)(P_Y P_Y^*)}$$

being P_X and P_Y the spectral power density estimators of signals X and Y, respectively. The asterisk denotes the complex conjugate. The estimation of spectral power was carried on with the Welch's method, using windows of 500 samples and overlap of 350 samples. Like the frequency spectrums, the coherence of the 10 s prior to the stimuli was subtracted to the coherence calculated in the 10s after the stimuli.

Spectral and coherence calculations were performed in Python language with the routines provided by the Scipy package. Wavelet spectrograms were performed using Python code freely available at https://github.com/patoorio/wavelets.

Multivariate Pattern Analysis (MVPA)

In addition to the univariate approach, multivariate spectral decoding was applied to the time–frequency data. This was done because MVPA decoding holds an advantage over most univariate methods as it offers more spatially sensitive dependent measures, demonstrating that information is present in activity patterns across brain regions [43,44]. The ADAM toolbox [43] was used on raw LFP data, which was transformed to time–frequency charts with similar settings epochs: 0 to 10 seconds after stimuli presentation, 1–40 Hz.

It is essential to keep a balanced number of trials between conditions when performing a multivariate decoding analysis since design imbalances may have unintended effects [43] on the linear discriminant analysis (LDA; the classification algorithm used here) and area under the curve accuracy metric (AUC; the accuracy performance metric used here). To keep a balanced number of trials across conditions, we randomly selected and discarded trials when necessary ('undersampling'; see Fahrenfort et al., 2018). We quantified classifiers' accuracy performance by measuring the AUC of the receiver operating characteristic (ROC), a measure derived from signal detection theory that is insensitive to classifier bias. AUC corresponds to the total area covered when plotting the cumulative true positive rates against the cumulative false positive rates for a given classification task. Thus, finding above-chance performance indicates that there was information contained in the neural data that the classifier decoded based on the stimulus features of interest.

LFP epochs time-locked to odorant presentation were classified according to their type (i.e., SE, AA, BS). Next, a backward decoding algorithm, using odorant category was applied according to a 10-fold cross-validation scheme. An LDA was used to discriminate between odorant classes after which classification accuracy was computed as the AUC, a measure derived from signal detection theory. AUC scores were tested per time point with double-sided t-tests across participants against a 50% chance level. These t-tests were double-sided and corrected for multiple comparisons using cluster-based 1000-iteration permutation tests [45] with a standard cut-off p-value of 0.05. This procedure yields time clusters of significant above-chance classifier accuracy, indicative of information processing.

Measurement of phase synchronization

We quantified phase locking between pairs of electrodes to measure dynamical interactions among electrode signals oscillating in the same frequency range. Phase synchronization analysis proceeds in two steps: the estimation of the instantaneous phases, and the quantification of the phase locking.

To obtain the instantaneous phases, φ, of the neural signals, we used the Hilbert transform. The analytic signal $\xi(t)$ of the univariate measure $x(t)$ is a complex function of continuous time defined as:

$$\xi(t) = x(t) + ix_h(t) = a_\xi(t)e^{i\varphi\xi(t)}$$

where the function is the Hilbert transform of:

$$x_h(t) = \frac{1}{\pi} P.V. \int_{-\infty}^{+\infty} \frac{x(t)}{t-\tau} d\tau$$

P.V. indicates that the integral is taken in the sense of Cauchy principal value. Sequences of digitized values give a trajectory of the tip of a vector rotating counterclockwise in the complex plane with elapsed time. The vector norm at each digitizing step t is the instantaneous amplitude $a_\xi(t)$:

$$a_\xi(t) = \sqrt{x(t)^2 + x_h(t)^2}$$

Similarly, the complex argument of analytic signal is the instantaneous phase $\varphi_x(t)$.

$$\varphi_x(t) = arctg \frac{ix_h(t)}{x(t)}$$

The instantaneous phase, although defined uniquely for any signal to which the Hilbert transform can be applied, is challenging to interpret for broadband signals. For this reason, a standard procedure is to consider only narrow-band phase synchronization by estimating an instantaneous phase for successive frequency bands, which are defined by band-pass filtering the time series[46]. Thus, we band-pass filtered LFP signals in multiple consecutive 1 Hz-wide frequency bins from 6 to 10 Hz using a zero-phase shift non-causal finite impulse filter.

Phase locking quantification: weighted phase lag index (wPLI)

Phase synchronization can be considered as an LFP/EEG measure of oscillatory coupling between neuronal populations[47,48]. The Phase Lag Index (PLI)[49] attempts to minimize the impact of volume conduction and common sources inherent in EEG data by averaging the signs of phase differences, thereby ignoring average phase differences of 0 or 180 degrees. This is based on the rationale that such phase differences are likely to be generated by volume conduction of single dipolar sources. Despite being insensitive to volume conduction, PLI has two important limitations: first, there is a strong discontinuity in the measure, which causes it to be maximally sensitive to noise; second, when calculated on small samples, PLI is biased toward strong coherences (i.e., it has a positive sample-size bias). Formally, the PLI is defined as the absolute value of the sum of the signs of the imaginary part of the complex cross-spectral density S_{xy} of two real-valued signals $x(t)$ and $y(t)$ at time point or trial t:

$$\mathrm{PLI} = \left| \frac{\sum_{t=1}^{n} sgn(imag(S_{xy,t}))}{n} \right|$$

The Weighted PLI measure (wPLI) [50] addresses the former problem by weighting the signs of the imaginary components by their absolute magnitudes:

$$\mathrm{wPLI} = \left| \frac{\sum_{t=1}^{n} |imag(S_{xy,t})| sgn(imag(S_{xy,t}))}{\sum_{t=1}^{n} |imag(S_{xy,t})|} \right|$$

The PLI sample size problem can be addressed by considering the same number of trials per condition in the phase coherence analysis. Further, wPLI represents a dimensionless measure of connectivity that is not directly influenced by differences in spectral or cross-spectral power. The wPLI index ranges from 0 to 1, with a value of 1 indicating perfect synchronization (phase difference is perfectly constant throughout the trials) and value 0 representing the total absence of synchrony (phase differences are random). Temporal evolution of wPLI was calculated using a 500 ms sliding window with 2 ms time step, i.e. with a 96% overlap between two adjacent windows. wPLI charts are expressed in z-scores (standard deviation units) relative to the pre-stimulus period (1 s) which was regarded as a baseline.

Information sharing between recording sites

We quantified the information sharing between electrodes by calculating the weighted symbolic mutual information (wSMI). This index estimates to which extent two LFP/EEG signals exhibit non-random joint (i.e., correlated) fluctuations. Thus, wSMI has been proposed as a measure of neural information sharing [51] and has three main advantages. First, it is a rapid and robust estimate of signals' entropy (i.e., statistical uncertainty in signal patterns), as it reduces the signal's length (i.e., dimensionality) by looking for qualitative or 'symbolic' patterns of increase or decrease in the signal. Second, it efficiently detects high non-linear coupling (i.e., non-proportional relationships between neural signals) between LFP/EEG signals, as it has been shown with simulated [48] and experimental EEG/LFP data [52]. Third, it rejects spurious correlations between signals that share a common source, thus prioritizing non-trivial pairs of symbols.

We calculated wSMI between each pair of electrodes, for each trial, after transforming the LFP signal into a sequence of discrete symbols defined by ordering of k time samples with a temporal separation between each

pair (or τ). The symbolic transformation is determined by a fixed symbol size (k = 3, i.e., 3 samples represent a symbol) and the variable τ between samples (temporal distance between samples), thus determining the frequency range in which wSMI is estimated [51,53]. We chose τ = 32. The frequency specificity f of wSMI is related to k and τ as follows:

$$f = \frac{1000}{\tau * k}$$

This formula, with a kernel size k of 3 and τ values of 32, produced a sensitivity to frequencies in the range ~6 to 10 Hz in which the peak of oscillatory activity is observed in the Power Spectral Density (PSD) (**Figure 2**). wSMI was estimated for each pair of transformed LFP signals by calculating the joint probability of each pair of symbols. The joint probability matrix was multiplied by binary weights to reduce spurious correlations between signals. The weights were set to zero for pairs of identical symbols, as these could have been elicited by a unique common source, and for opposite symbols (i.e., of in opposite direction), as these could reflect the two sides of a single electric dipole. The following formula calculates wSMI (in bits, but shown in arbitrary units or AU, with absolute values):

$$wSMI(X,Y) = \frac{1}{\log(k!)} \sum_{x \in X} \sum_{y \in Y} w(x,y)\, p(x,y) \log\left(\frac{p(x,y)}{p(x)p(y)}\right)$$

Here, x and y are symbols present in signals X and Y respectively; w(x,y) is the weight matrix and p(x,y) is the joint probability of co-occurrence of symbol x in signal X and symbol y in signal Y. Finally, p(x) and p(y) are the probabilities of those symbols in each signal and k! is the number of symbols used to normalize the mutual information by the signal's maximal entropy. Temporal evolution of wSMI was calculated using a 500ms sliding window with 2-ms time step, i.e., with a 96% overlap between two adjacent windows.

Co-Information between recording sites

For each trial, after band-pass filtering the LFP signals between 6 to 10 Hz, we computed the time-resolved spectral power by computing the square of the instantaneous amplitude $a_\xi(t)$ using the Hilbert transform procedure described above. Using this resulting signal (i.e., the time-resolved spectral power), we then computed the co-Information (co-I). The co-information (co-I) [54,55] has been calculated in the following way:

$$coI(X;Y;S) = I(X;S) + I(Y;S) - I(X,Y;S)$$

For each time point, *I(X;S)* corresponds to the mutual information (MI) between the signal at recording site *X* and stimuli class *S*. *I(Y;S)* corresponds to the MI between the signal at recording site *Y* and stimuli class *S*. Finally, *I(X,Y;S)* corresponds to the MI between stimuli class *S* combining signals from recording sites *X* and *Y*. This way, co-information was computed for each pair of odorants between all three pairs of recording sites.

Positive co-information means that signals between recording sites contain redundant, or overlapping, information about the stimuli. Negative co-information corresponds to synergy between the two variables. This means that the mutual information when considering the two variables jointly is larger than considering the variables separately.

Statistical Analysis

Statistical analyses were performed using MATLAB (2016a), Jamovi (Version 0.8.1.6) [Computer Software] (Retrieved from https://www.jamovi.org) (open source), and JASP Team (2018; JASP; version 0.8.4 software) statistical software.

RESULTS

General description of the electrical responses

To retest the still unanswered hypothesis if odor information is carried by LFP oscillations from the olfactory bulb to higher olfactory centers, we recorded olfactory responses as reflected by variations of the LFP to four different types of odors: Two synthetic mixtures, amino acids and bile salts, one natural mixture resulting from the mechanical maceration of conspecific skin, and the individual synthetic odorant PEA. Recordings were obtained simultaneously from the olfactory epithelium, the olfactory bulb and two principal olfactory centers of the telencephalon: The subpallial ventral nucleus of the ventral region (Vv) and the pallial posterior dorsal region (Dp) (**Figure 1A**). Odor stimulation, as opposed to trout water (TW, control), always generated a dose-dependent negative EOG, and a transient and near-simultaneous increase in LFP oscillation amplitudes in the olfactory bulb and the telencephalic olfactory areas, lasting 10 to 15 s (**Figure 1B-E**). To test if repeated trials affected the LFP oscillations through sensory adaptation, sensitization or learning-related mechanisms, we compared the responses of 20 consecutive trials, spaced 50s apart, to the same stimuli (**Figure 1B'-E'**). Interestingly, the amplitudes of the oscillatory responses and the response envelopes remained unaltered throughout the trial sequence in the OB, and the telencephalic areas Vv and Dp. These findings allowed us to pool the data from several consecutive trials for subsequent analyses.

Analysis of LFP oscillations in the OB, and telencephalic areas Vv and Dp

We characterized the frequency-domain characteristics of the electrophysiological recordings and the responses to odorants, using the Welch periodogram method (**Figure 2A-B**). To improve the signal-to-noise ratio, we averaged the spectra across trials of the same experiment. Figure 2A shows the average spectrum calculated from a 10s window before (dotted line) and after (continuous line) exposure to the amino acid mixture (AA), while recording in Vv. The baseline activity contains prominent low-frequency (<7 Hz) activity, and thus the baseline spectrum was subtracted from the odorant response spectrum (**Figure 2A, inset**). This subtraction was performed on all data shown in **Figures 2 and 3**. **Figure 2B** shows the average of the spectra for all experiments and their recordings in OB, Vv and Dp, while exposed to AA, SE, BS and PEA. Controls with trout water are shown in blue. AA, SE and BS evoked strong oscillatory responses in the recorded brain areas in the 5-9 Hz band, albeit with different magnitudes. The response to PEA, however, failed to generate a robust oscillation in most experiments. We hypothesize that this is due to PEA, a component of floral odors, being a novel odorant for the trouts, with no or little biological meaning. Therefore, the responses to PEA were excluded from the following frequency-domain analyses.

The frequency of the maximum amplitude for each experiment is displayed in the insets. Notably, the response to BS appears to occur at a higher frequency on average than the response to AA and SE. However, only at OB and Dp a significant difference in the maximum frequencies was detected (Kruskal-Wallis test: OB H=6.43,

p=0.04; Dp H=7.84, p=0.02; Vv H=1.75, p=0.42), and the difference was only found between AA and BS (Dunn's posthoc test: OB AA/SE p=0.52, AA/BS p=0.013, SE/BS p=0.06; Dp AA/SE p=0.21, AA/BS p=0.005, SE/BS p=0.11).

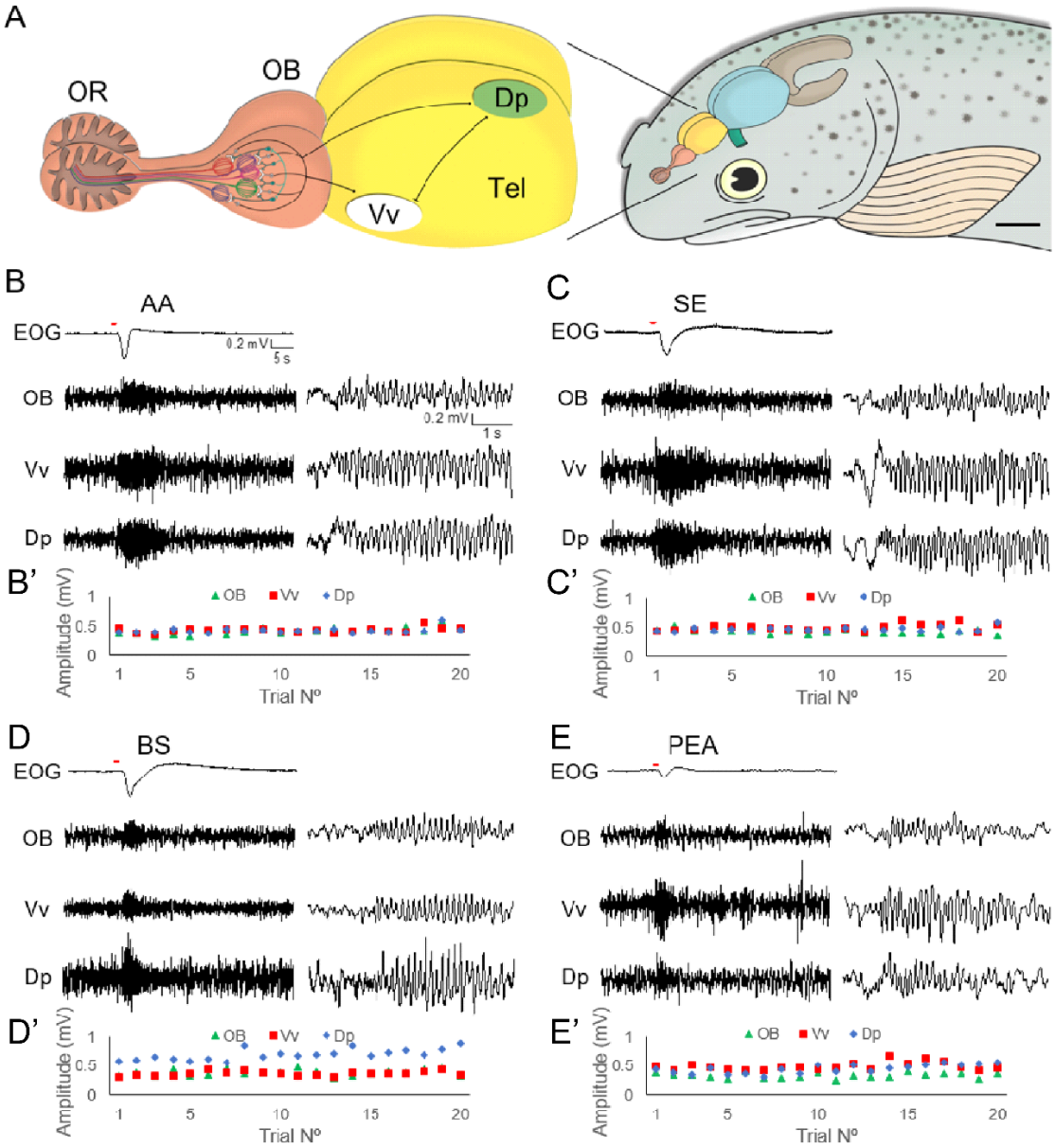

Figure 1. Recording sites and raw simultaneous recordings of the EOG and LFP oscillations from the olfactory bulb (OB), the ventral nucleus of the ventral telencephalon (Vv) and the dorsal posterior zone of the telencephalon (Dp). (**A**) Schematic drawing of the rainbow trout forebrain. Olfactory information and LFP oscillations of different frequency bands are transmitted in parallel from the olfactory bulb to higher olfactory areas of the telencephalon, notably Vv and Dp. Scale bar: 3 mm. (**B-E**) Responses to an amino acid (AA, 100 µM) and a bile salt (BS, 700 µM) mix, conspecific skin extract (SE, diluted 1:500) and beta-phenylethyl alcohol (PEA, 100 µM) were recorded simultaneously from OB, Vv and Dp, showing prominent and ostensibly synchronous oscillatory activity during odor stimulation. The sets of traces to the right display details on a shorter timescale. (**B'-E'**) Oscillatory response amplitudes remained stable for 20 trial repetitions in each olfactory brain area, showing no sign of sensory adaptation.

To analyze the time-dependent frequency components of the response, we analyzed the recordings using a continuous Morlet wavelet transform. As previously, the transforms were averaged for all sweeps in every single experiment, and the frequency components prior to stimulus exposure were subtracted. In this case, the results

are expressed as z-score (see Materials and Methods). **Figure 2C** shows a spectrogram of the response recorded at the OB after exposure to BS, where the maximum frequency of the oscillation suffers a shift towards lower frequencies as the response progresses in time.

Although in many recordings the response extended past 5 s (sometimes reaching up to 10 s), the most robust and consistent responses were localized in the 1.5 to 4 s window. We calculated the average maximum frequency for that time span, shown in **Figure 2D**. All responses to AA, SE and BS show the same frequency shift, starting at a higher frequency and then decreasing in about 2Hz after 2 s. Interestingly, this analysis shows more evidently that BS evokes oscillations at a higher frequency than the other odorants.

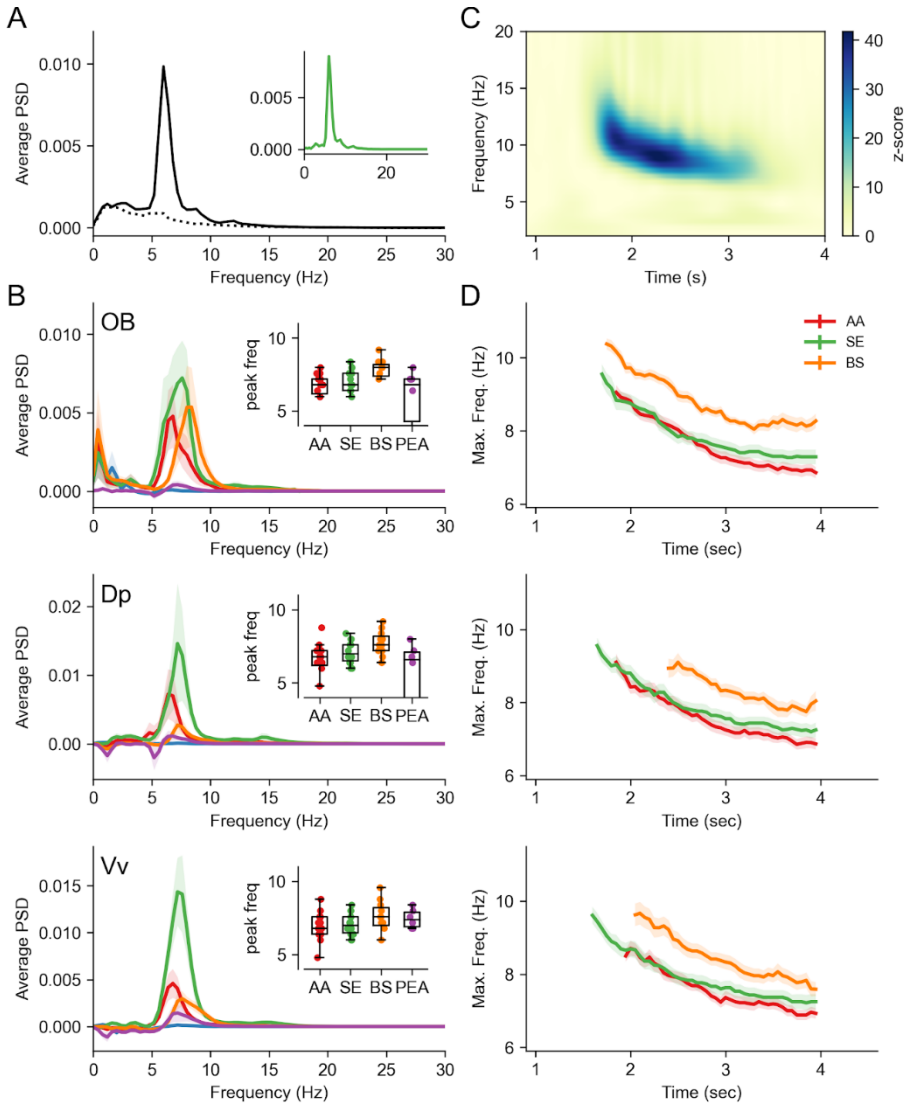

Figure 2. Oscillatory characteristics of neural response to odorants. (**A)** Average frequency spectrum of the LFP response recorded in Vv, upon exposure to the AA mix. Dotted line is the spectrum of the recording prior AA exposure (10 s) and the continuous line corresponds to the 10 s after exposure to AA. The spectra of 20 repetitions were averaged. The inset shows the net response to the odorants (baseline subtracted). (**B)** Average of baseline-subtracted spectra of the responses from OB, Vv, and Dp when stimulated with AA, trout skin extract (SE), bile salts (BS) and PEA, in addition to trout water control (TW; blue line). The average spectra of 11-14 experiments per condition are shown, with the mean as continuous line and the standard error as colored shade. The inset shows the peak of the response spectra. (**C)** Wavelet spectrogram of oscillations recorded from the OB upon exposure to SB at time t = 0s. The data are expressed as z-score with respect to the

baseline activity at each frequency during the 10 s prior to the stimulus. As in (A), it represents the average of 20 trials repeated in the same specimen with the same stimulus. (**D)** Average (lines) and standard error (shadow) of the maximum frequency at each time point, according to the wavelet spectrogram. The average was calculated only at times when more than half of the experiments showed a z-score higher than 5 in any frequency within the 5-20 Hz range, thus the different durations of the responses. Maxima were obtained from baseline-subtracted spectrograms.

We next employed frequency-domain analysis to assess the degree of synchrony between the oscillations in different areas, by calculating the coherence cross-spectra. **Figure 3A** shows the average coherence spectra of the responses recorded in presence of AA, SE and BS, for the three possible pairs between OB, Vv and Dp. All responses displayed a strong coherence with a peak around 7-8 Hz, the same frequency of the main oscillation. The median frequency of the maximum coherence (insets) was not significantly different between groups (Kruskal-Wallis test, OB-Dp H=2.62 p=0.27; OB-Vv H=4.4 p=0.11; Dp-Vv H=5.25 p=0.07). Interestingly, AA and SE also generated coherence in the 15Hz range, although this oscillation was not particularly visible in the frequency spectra. Most likely, this reflects harmonic components of the main oscillation frequency.

Finally, we analyzed the phase component of the cross-spectra at the frequency of highest coherence between areas (**Figure 3B)**. Although there is variability between experiments, on average the oscillation in Dp leads the activity in OB by 1/4 of a cycle (~35 ms at 7Hz). Alternatively, OB leads the oscillations in Dp by 3/4 of a cycle or ~100 ms. This tendency is more marked for the response to AA and SE than to BS. Also, on average the responses in OB and Vv are in anti-phase, equivalent to a lag of ~70 ms at 7Hz. Finally, the phase relationship between Dp and Vv is the most variable of all, but the tendency is for Vv to lead Dp by 1/4 of a cycle.

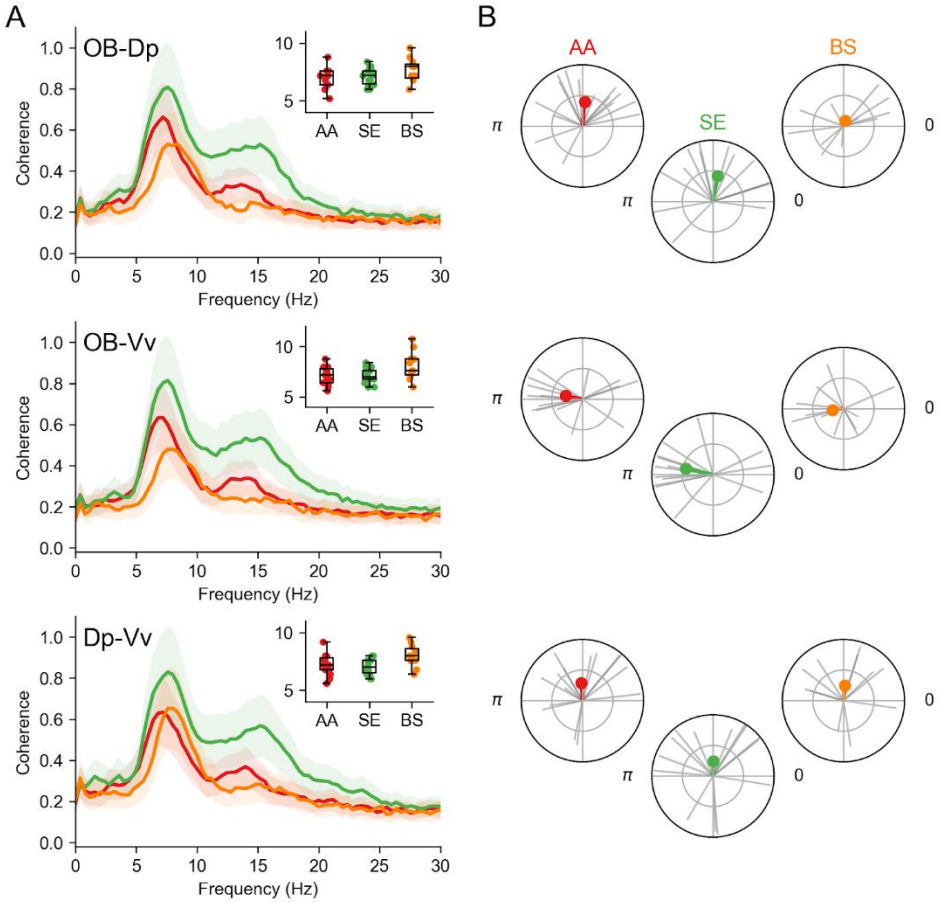

Figure 3. Coherence in the oscillatory response recorded in different regions. (A) Coherence spectra showing the mean (lines) and standard error (shades) of coherence detected at every frequency, in the pairs of regions indicated and after exposure to the odorants that evoked the most robust responses. For each experiment, a coherence spectrum was calculated and the experiments for each odorant were averaged. Inset shows the frequency where the peak of the coherence was detected. **(B)** Phase of the coherence measured at the frequency of maximum coherence. The gray lines denote the amplitude (radius) and phase (angle) of the complex-valued coherence corresponding to the frequency at the maximum for each individual experiment. Colored lines and dots represent the average vector across experiments performed with the same odorant.

Thus, the basic characteristics of the odor-elicited oscillations allow for little or no discrimination between odorants. The only exception seems to be the higher frequency of oscillations elicited by bile salts.

Multivariate spectral decoding of LFP oscillations across OB, Vv and Dp

Is the spatial information across regions relevant for odorant discrimination? To determine whether a spatially extended pattern of oscillatory activity underlies olfactory discrimination, we performed a spectral Multivariate Pattern Analysis (MVPA or "spectral decoding"; King and Dehaene, 2014). Spectral decoding allows to obtain a measure of odorant discrimination without having to a priori specify at which areas or frequency bands these differences emerge, while at the same time extracting subtle trial-by-trial neural differences that are undetected by standard averaging procedures (**Figure 4A**) like those performed in the univariate analyses described in the previous section (Fahrenfort et al., 2018). To do so, we trained a classifier to simultaneously distinguish the three types of odorants across the three regions (OB, Dp and Vv) (**Figure 4B**; see Materials and Methods). Above-chance classification accuracies imply that the relevant information about the decoded odorants is present in the oscillatory activity, implying spatially distributed olfactory processing and coding.

Interestingly, and contrary to the univariate spectral analyses performed above, multivariate decoding showed that information about the three odorant categories was reliably decoded above chance when the spatial variation in neural activity across regions was considered (**Figure 4B**, right panel). A cluster-based permutation test showed a significant cluster of increased classification accuracy spanning several frequencies and time points (cluster $p < 0.01$; peak frequency: 6-10 Hz; time range: 1 to 9 secs). This result suggests that the relevant information for odorant discrimination is encoded by the functional interaction between olfactory regions.

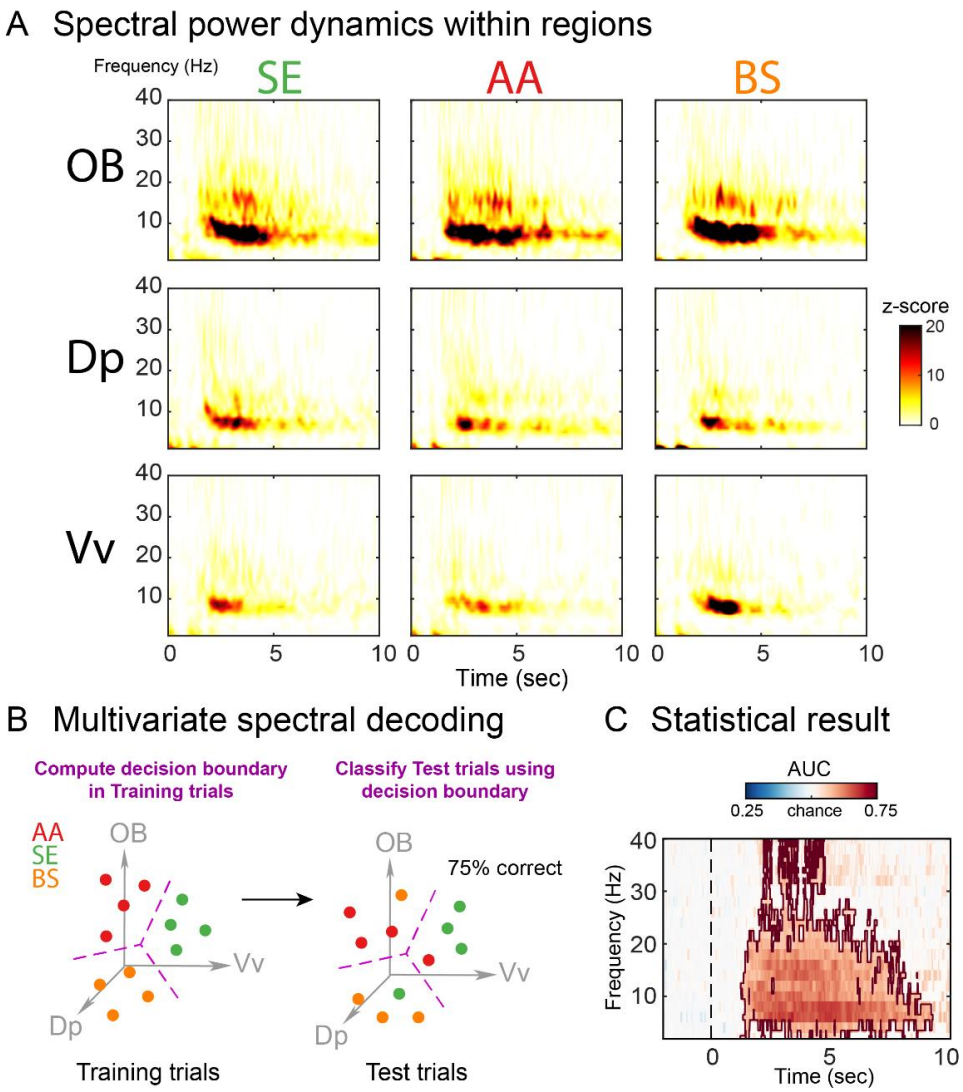

Figure 4. Spectral decoding across OB, Vv and Dp. (A) Temporal dynamics of spectral power. Time-frequency charts were averaged across individuals per odorant and region. **(B)** Multivariate spectral decoding. Each region is considered as a separate dimension, or "feature", in a N-dimensional space, depicted by the 3-dimensional axes conformed by OB, Vv and Dp regions (in grey). Each trial-wise odorant presentation (AA in red, SE in green, and BS in orange) produces a pattern that occupies a point in a 3-dimensional neural activation space. A linear classifier (LDA) learns a way to transform this high-dimensional space into a new one in which the channel patterns associated with each odorant are separable by a decision boundary (*left panel*). LDA assigns an odorant label for the training data based on the position of the activity patterns relative to the decision boundary. The performance of the classifier is then a function of the accuracy of its label assignments (e.g., percentage correct, *middle panel*). **(C)** This procedure is performed at each time point and frequency and a cluster-based permutation test ($p<0.05$; brown boundary) was performed to determine significant decoding above chance (see Materials and Methods).

Information sharing between OB-Vv, OB-Dp, and Vv-Dp across odors and control

Functional connectivity – understood as the coordinated activity across brain areas – is a key element of several theories of perception across species (Fries 2005; Saalmann et al. 2012; King et al. 2013; Bastos and Schoffelen 2016). While classic metrics of functional connectivity such as phase coherence investigate the temporal synchronicity between stereotypical patterns observed in the LFPs (i.e., neural oscillations), metrics based on information processing capture dynamics that are not necessarily periodic or oscillatory [51]. Importantly, non-oscillatory or 'aperiodic' information is critical for establishing distributed functional connectivity when brain

signals are highly complex [48]. Experimentally, non-oscillatory functional connectivity can be investigated by computing the shared information across brain regions, showing its robustness in discriminating perceptual representations [52,59] and alertness states [48,51,53]. Based on these previous findings and on the spectral decoding results (**Figure 4**), we reasoned that a mechanism based on distributed information sharing across OB, Vv and Dp could be appropriate for distinguishing odor composition and intensity. Thus, we applied a method for quantifying non-oscillatory functional connectivity based on information theory: weighted symbolic mutual information (wSMI) [51].

For each odorant category used here, we computed information sharing between regions in the frequency range of the oscillatory response (~6-10 Hz; **Figure 5**). We first computed wSMI between OB and Vv (**Figure 5A**). Kruskal-Wallis test showed a significant interaction across odors (odors: TW, AA, BS, SE; X^2 = 29.9, p<0.001). Post-hoc comparisons showed differences between odors and control (AA-TW: W = 5.85; p<0.001, SE-TW: W = 5.97, P<0.001, BS-TW: W = 4.80, p<0.001), and between two out of three odors (AA-SE: W = 3.52, p = 0.013; SE-SB: W = -3.78, p = 0.007; AA-SB: W = -1.81, p = 0.20). A similar interaction effect across odors was observed in wSMI between OB and Dp (**Figure 5B**; Kruskal-Wallis test: X^2 = 28.0, p<0.001), with significant post-hoc effects between odors and control (AA-TW: W = 5.92; p<0.001, SE-TW: W = 5.49, P<0.001, BS-TW: W = 4.53, p<0.001), and between two odors (AA-SE: W = 3.46, p = 0.014; SE-SB: W = -3.78, p = 0.007; AA-SB: W = -2.29, p = 0.10). Interestingly, in the case of the wSMI between Vv and Dp (**Figure 5C**), we observed a significant interaction and simple effects across the three pairs of odors (Kruskal-Wallis test: X^2 = 29.2 p<0.001; Post-hoc comparisons: AA-SE: W = 3.68, p = 0.009; SE-SB: W = -3.84, p = 0.007; AA-SB: W = -2.89, p = 0.032), and between odors and control (AA-TW: W = 5.38; p<0.001, SE-TW: W = 5.97, P<0.001, BS-TW: W = 4.90, p<0.001).

Phase synchrony between OB-Vv, OB-Dp, and Vv-Dp across odors and control

In order to compare our results with a classical functional connectivity metric, we performed a phase synchronization analysis using the weighted phase lag index (wPLI) due its robustness to volume conduction, common source and muscular artifacts [50]. In a similar manner as with wSMI analyses, we computed the phase synchronization between pairs of regions for each odorant in the frequency range (6-10 Hz) of the oscillatory response (**Figure 6**).

In the case of wPLI between OB and Vv (**Figure 6A**), although the Kruskal-Wallis test showed a significant interaction across odors (X^2 = 11.9, p = 0.008), post-hoc comparisons revealed no differences between odors (AA-SE: W = 2.13, p = 0.132; SE-SB: W = -2.18, p = 0.122; AA-SB: W = -0.42, p = 0.763), and only two odors were different from control (AA-TW: W = 3.67; p = 0.009, SE-TW: W = 4.21, P = 0.003, BS-TW: W = 2.61, p = 0.065). In the case of wPLI between OB and Dp (**Figure 6B**), a Kruskal-Wallis test showed a significant interaction across odors (X^2 = 22.0 p<0.001) and between odors and control (AA-TW: W = -5.27; p < 0.001, SE-TW: W = -5.49, p <0.001, BS-TW: W = -4.05, p = 0.004). However, no differences were observed between odors (AA-SE: W = 2.07, p = 0.142; SE-SB: W = -2.13, p = 0.132; AA-SB: W = -0.80, p = 0.572). Similar results were obtained in the case of wPLI between Vv and Dp (**Figure 6C;** Kruskal-Wallis test: X^2 = 22.3 p<0.001), with differences between odors and control (Post-hoc comparisons: AA-TW: W = 5.11; p <0.001, SE-TW: W = 5.54, p <0.003, BS-TW: W = -4.37, p = 0.002), but not between odors (Post-hoc comparisons: AA-SE: W = 2.45, p = 0.083; SE-SB: W = -2.66, p = 0.060; AA-SB: W = -0.58, p = 0.679).

Altogether, these results suggest that the feature of the oscillatory response relevant for odorant discrimination is the shared information across regions and not the phase synchronization between them.

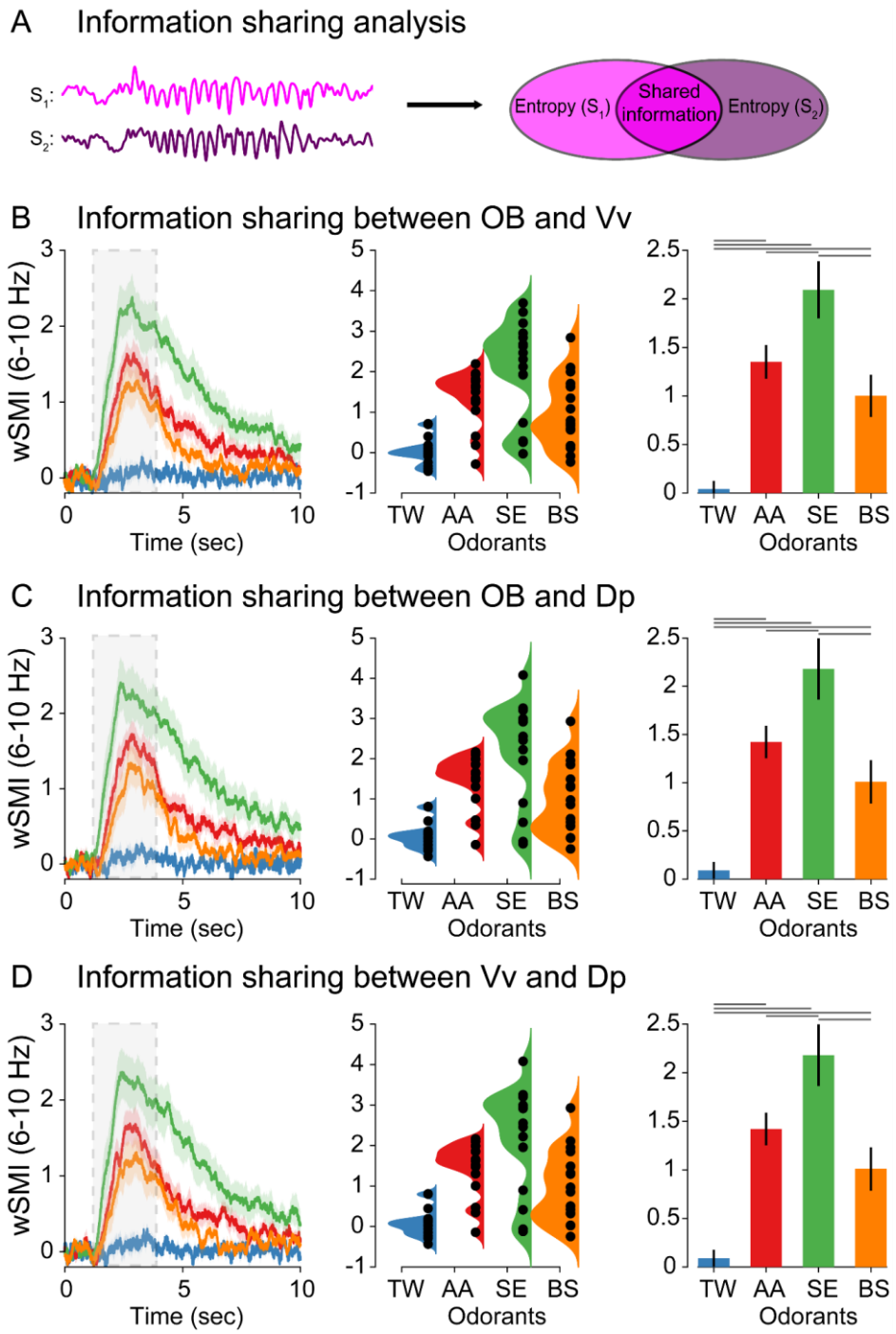

Figure 5. Mutual information between OB-Vv, OB-Dp and Vv-Dp. (A) Schematic representation of wSMI analysis (i.e., mutual information). After the symbolic transformation (see Materials and Methods), entropy of signals S_1 (purple oval) and S_2 (pink oval) are computed separately, and then their mutual information (overlapping purple oval) represents the shared odorant information between areas. wSMI dynamics between OB-Vv **(B)**, OB-Dp **(C)**, and Vv-Dp **(D)** in the ~6-10 Hz range for each odorant (left panel), the single-animal distribution of values during the 1-5 sec range (middle panel) and its group statistical analysis (right panel; *post-hoc* differences depicted as gray lines above the corresponding odorants). RANOVA revealed a significant interaction effect of wSMI between odorants and control (TW), and between most of the odorants after the *post-hoc* contrasts (see Results section).

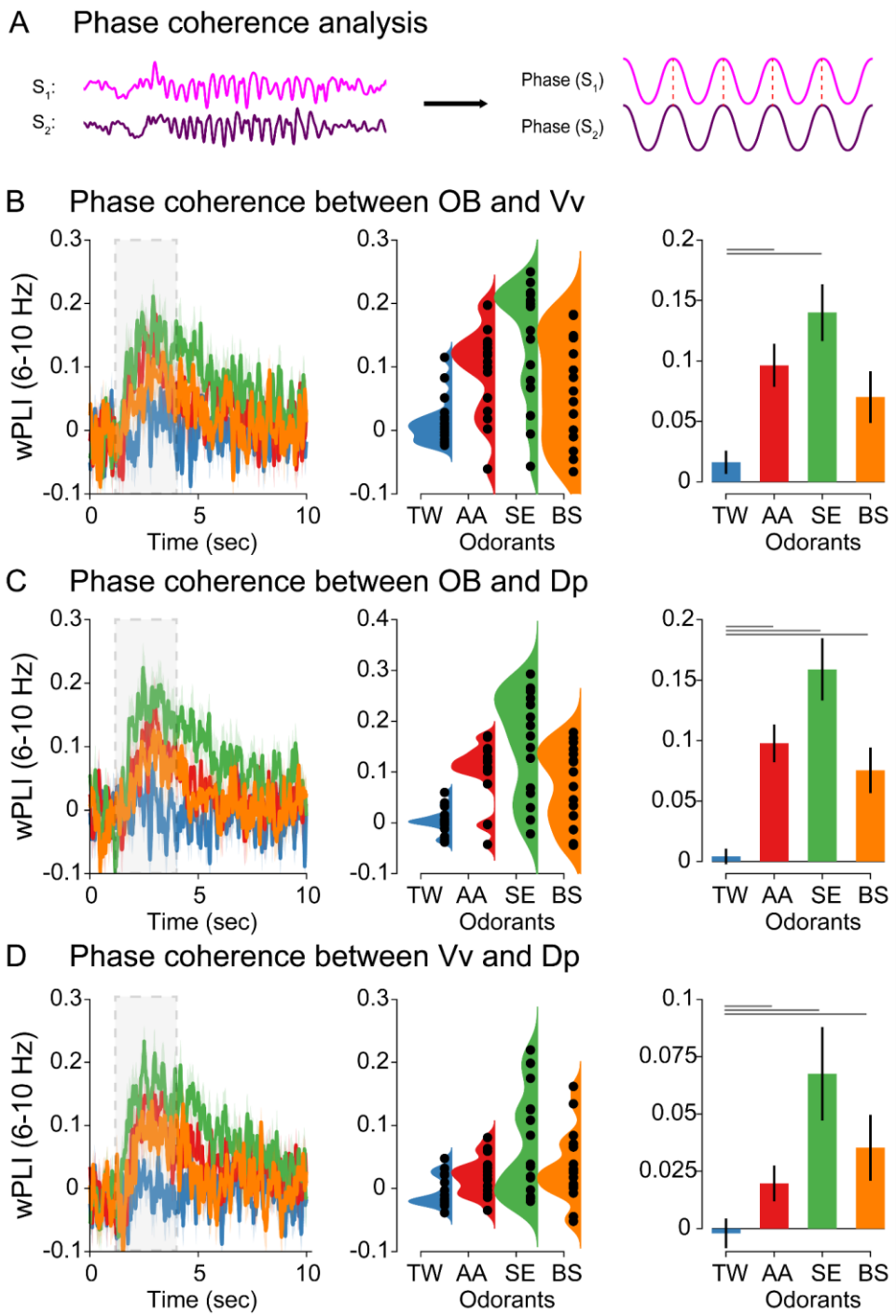

Figure 6. Phase coherence between OB-Vv, OB-Dp and Vv-Dp. (A) Schematic representation of wPLI analysis (i.e., phase coherence). After filtering the signal in a selected frequency range (see Materials and Methods) the instantaneous phase is computed for both signals S_1 (pink) and S_2 (purple), and the phase difference between them (red dashed line). In this example, phase difference between signals remains constant across time, representing a highly phase-coherent pair of neural signals. wPLI dynamics between OB-Vv **(B)**, OB-Dp **(C)**, and Vv-Dp **(D)** in the 6-10 Hz range for each odorant (left panel), the single-animal distribution of values during the 1-5 sec range (middle panel) and its group statistical analysis (right panel; *post-hoc* differences depicted as gray lines above the corresponding odorants). RANOVA revealed a significant interaction effect between in wPLI odorant and control (TW), but no differences between pairs of odorants were observed after *post-hoc* comparisons (see Results section).

Information redundancy between Ob, Vv and Dp.

Robustness, understood as the ability of tolerating perturbations that might affect the system's functionality, is a desirable characteristic for the olfactory system [60], for instance to preserve odorant discriminability in the presence of noise, high background or highly variable odor plumes. Although wSMI provides relevant insight into the *amount* of information shared between brain regions to distinguish odorant identity, it does not provide any insight into whether the brain regions are processing the same or different information. Thus, in order to investigate robustness from an informational point of view, we need a more nuanced analysis capable of quantifying the *redundant* information that is being processed between regions [61]. Observing redundancy between brain regions would be an indication of the system's robustness, as different brain regions can perform the same function (i.e., odor mix decoding).

Odorant information in two brain regions can be schematized in a Venn diagram (**Figure 7A**). The first quantity of interest is the overlap, termed *redundancy* (left panel, red area). Each inner circle represents the mutual information between pairs of odorant categories and their LFP signals (e.g. between AA and EPT) for an individual brain region (e.g. Vv). Conceptually, the term redundancy refers to the case in which the information conveyed by region A and region B is the same (e.g. Vv and Dp). If the variables are redundant, each brain region *alone* is sufficient to convey all the information about odorant category, and adding observation from the second brain region does not contribute additional information. On the other hand, the concept of *synergy* is related to whether region A and B convey *extra* information about odorant identity only if both regions are considered jointly (right panel, blue area). Redundancy and synergy are reflected by *positive* and *negative* values of co-information, respectively (see Materials and Methods).

Interaction information analysis revealed positive values, signaling information redundancy, between the post-stimuli and pre-stimuli periods (PSP). This effect was observed for all odorant pairs and between all brain regions implicating that the information between olfactory brain areas analyzed here is redundant (Ob-Vv: AA-EPT vs PSP, W = 13.86, p<0.001; EPT-SE vs PSP, W = 17.96; p<0.001; AA-SE vs PSP, W = 14.50, p<0.001; Ob-Vv: AA-EPT vs PSP, W = 12.78, p<0.001; EPT-SE vs PSP, W = 16.23; p<0.001; AA-SE vs PSP, W = 13.21, p<0.001; Ob-Vv: AA-EPT vs PSP, W = 17.01, p<0.001; EPT-SE vs PSP, W = 14.20; p<0.001; AA-SE vs PSP, W = 15.39, p<0.001).

Interestingly, the dynamics of redundancy was not the same for different pairs of odorants. For each pair of odorants, we computed the interaction information between a pair of brain regions in the frequency range of the oscillatory response (~6-10 Hz; **Figure 7**). Interaction Information was first computed between OB and Vv (**Figure 7A**). Kruskal-Wallis test showed a significant interaction across difference in odor pairs (pairs: AA-EPT, EPT-SE, AA-SE; X^2 = 13.2, p=0.001). Post-hoc comparisons showed differences between odor pairs (EPT-SE vs AA-EPT: W = 2.77, p<0.050; AA-SE vs EPT-SE: W = -4.74, p<0.001; AA-SE vs EPT-SE: W = -3.09, p = 0.029). A similar interaction effect across differences in odor pairs was observed between OB and Dp (**Figure 7B**; Kruskal-Wallis test: X^2 = 9.81, p=0.007), with significant post-hoc effects between one odor pair of odor differences (EPT-SE vs AA-EPT: W = 2.13, P = 0.132; AA-SE vs EPT-SE: W = -4.37, p = 0.002; AA-SE vs EPT-SE: W = -2.35, p = 0.097). Interestingly, in the case of the wSMI between Vv and Dp (**Figure 7C**), we observed a significant interaction and simple effects across the three pairs of odor differences (Kruskal-Wallis test: X^2 = 16.8, p <0.001; Post-hoc comparisons: EPT-SE vs AA-EPT: W = 3.09, p = 0.029; AA-SE vs EPT-SE: W = -5.49, p < 0.022; AA-SE vs EPT-SE: W = -3.25, p < 0.001).

Taken together, these results indicate that the type of interactions observed between recording sites is informationally redundant between each other, suggesting that the ability to reliably discriminate different odorants is robustly implemented by the different components of the olfactory system.

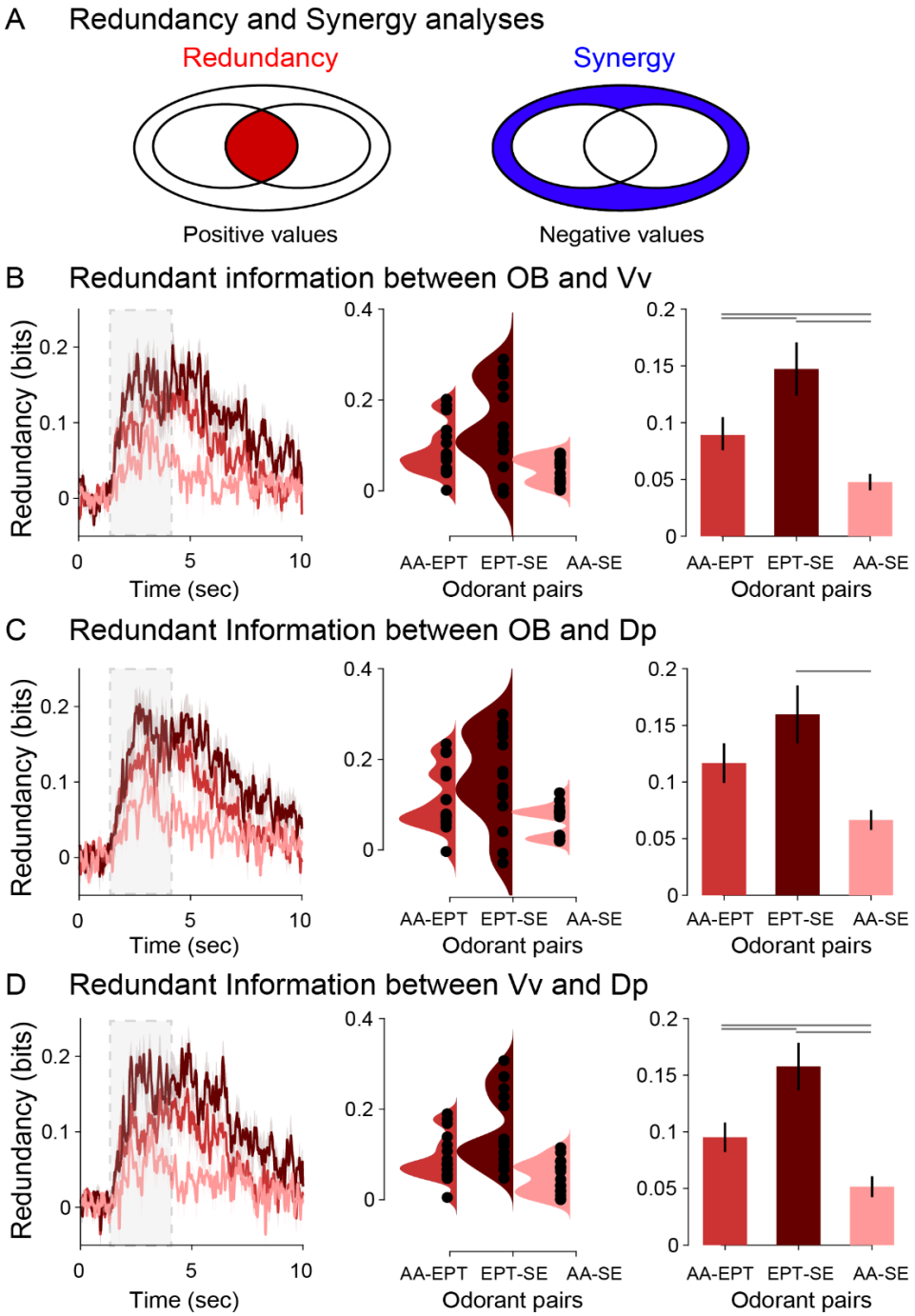

Figure 7. Redundancy between OB-Vv, OB-Dp and Vv-Dp. (A) Schematic representation of redundancy and synergy analyses. Each inner circle represents the mutual information between LFP signals of a pair of odorants for an individual brain region, and the overlapping region represents the redundancy (red; left panel). The outer circle represents information that is synergistic (blue; right panel). Redundancy dynamics between OB-Vv **(B)**, OB-Dp **(C)**, and Vv-Dp **(D)** in the ~6-10 Hz range for each odorant (left panel), the single-animal distribution of values during the 1-5 sec range (middle panel) and its group statistical analysis (right panel; *post-hoc* differences depicted as gray lines above the corresponding odorants).

DISCUSSION

We have shown that primary response parameters such as oscillatory power, main frequency, time course and phase were robust but largely uninformative to vastly different olfactory stimuli when recording sites were analyzed separately. Conversely, we were able to reliably establish odor identity when recording sites were considered together using advanced decoding techniques, and when the amount and type of information shared between the recording sites was established. Our results suggest that distributed information across the olfactory system indexes odorant identity.

In the mammalian olfactory bulb, seminal studies conducted on behaving animals have demonstrated that neural activity at different spatiotemporal scales is modulated by animal behavior and experience apart from properties of the olfactory stimuli. For instance, in rabbits, amplitude-modulated patterns across 64 electrode arrays implanted in the OB exhibited highly context-dependent LFP oscillations during sniffing[62]. Similarly, single-cell mitral and tufted cells were strongly influenced by contextual efferent inputs in behaving rats[63]. These studies suggest that LFP patterns in the OB contain a significant amount of non-primary sensory information, likely reflecting experience, the behavioral context, and associated information apart from primary characteristics of the stimulus.

If these studies account for the effects of context and behavior on olfactory processing, then what are the neural markers associated with odorant properties themselves? We sought to answer this question using anesthetized trout, allowing us to control for confounding factors such as respiration and sniffing, movement, experience, and learning. Interestingly, spectral decoding and information-based connectivity analyses showed that the spatially distributed oscillations carry information relevant for odorant discrimination. We interpret the shared information conveyed in the LFP activity across OB, Dp and Vv as reflecting the complexity of the odor mixture. Arguably, stimuli formed by complex mixtures with diverse molecular structures should elicit a neural response containing a higher diversity of information patterns (i.e., higher signal entropy), resulting in an increase in information sharing between olfactory brain areas when they are co-activated.

The stimuli used in this study are blends of various odorants displaying different levels of complexity based on the quantity and diversity of their components (see Materials and Methods). Thus, the mixture of bile salts (BS) is composed of 4 compounds and the mixture of amino acids (AA) is composed of 5 amino acids. On the other hand, skin extract (SE), as a mixture resulting from the homogenization of a complete biological tissue, is composed of hundreds of compounds, many of them difficult to identify, conveying much greater complexity compared to AA and BS[42]. Although it cannot be directly concluded that the properties of the molecules that make up BS and AA determine greater or lesser complexity as both are mixtures of few compounds, the amount of their components can be arguably used as a proxy for structural complexity. Supporting this view, in all three pairs of regions, the wSMI results showed a correspondence between the quantity of components present in each odor, and the amount of information sharing between regions (**Figure 5B-C-D**). Thus, while SE showed the highest wSMI value (green bar; right panel), BS showed the lowest apart from control (yellow bar; right panel), and AA showed intermediate values (red bar; right panel). This correspondence between odor complexity – in terms of number of components – and the amount of information sharing between OB, Vv and Dp suggest that at least some of the information captured by wSMI encodes structural properties of the stimuli across the olfactory system.

Why does the information-based connectivity metric (wSMI) capture odorant identity while the spectral-based connectivity measure (wPLI) does not? As described in the introduction, studies of LFP activity in the olfactory system have mainly focused on periodic or 'rhythmic' neural oscillations manifested as spectral peaks at different frequency bands (e.g. beta and gamma). However, the spectrum of mesoscopic electrophysiological signals (e.g., LFP, EEG) also contains aperiodic or 'arrhythmic'[64–66] that have been related to the integration of underlying synaptic currents[67]. Problematically, the standard approach of analyzing periodic power or phase synchronization (e.g., wPLI) through band-pass filtering confounds both periodic and aperiodic activity[68]. If we observed spectral changes between two conditions (e.g., between two odorants) due to aperiodic activity, comparing bandpass-filtered neural oscillations would confound or hide the aperiodic components of these spectra.

Crucially, the aperiodic component of the signal can be investigated using wSMI – an information-theoretic connectivity metric[48,51]. For instance, using realistically simulated EEG signals, we have recently demonstrated that wSMI can reliably detect aperiodic, non-linear interaction across brain regions that phase synchronization (i.e., wPLI) was unable to detect [48]. The olfactory areas investigated in this study are thought to perform different roles during olfactory discrimination. While the OB is thought to decode the odorant's molecular structure, higher olfactory centers such as Dp and Vv are thought to process more contextual and behaviorally relevant information such as feeding, reproduction, and danger sensing[69]. We propose that the associations between lower (OB) and higher (Dp and Vv) centers are established by a mechanism of information exchange conveyed by the aperiodic component of the olfactory oscillation.

Robustness is a functional consequence of degenerate systems, that is, systems conformed by structurally different elements capable of performing the same function[70–72]. Robustness is ubiquitous across many biological systems including neural circuits and networks[70,72,73]. Crucially, robust systems are also capable of preserving their functions when exposed to changes in contextual circumstances, making them extremely resilient. From an evolutionary point of view, it is reasonable to conceive that selection processes such as those underlying the evolution of the olfactory system favor the development of robust systems. Phylogenetically, a mechanism preserving the implementation of the same function by different brain regions might serve a crucial evolutionary function: making olfactory discrimination quickly adaptable to changes in the environment.

We have used information redundancy analyses to characterize the robustness of the teleost olfactory systems in implementing odorant discrimination. There is mounting evidence that redundancy in neural networks may provide various computational benefits, for example, enabling stable computations despite unstable neural dynamics[74–76] and allowing the central nervous system to filter out unwanted noise[77]. Our finding of increased information redundancy across recording sites suggest that although neuroanatomically divergent, the underlying neural circuits of OB, Vv and Dp can process the same information about odorant identity, supporting the idea that – at least under anesthetized conditions – the olfactory system of teleost is functionally robust.

In conclusion, our results indicate that primary response parameters such as oscillatory power, main frequency, time course and phase were robust but largely uninformative to vastly different olfactory stimuli when recording sites were analyzed separately. However, a more nuanced analytical approach investigating the information relationship between recording sites revealed shared information critical for olfactory discrimination, supporting the notion that olfactory oscillations are carriers of information about odorant identity across olfactory brain centers.

REFERENCES

1. Adrian ED, Ludwig C. Nervous discharges from the olfactory organs of fish. *J Physiol*. 1938. doi:10.1113/jphysiol.1938.sp003693
2. Adrian ED. Olfactory reactions in the brain of the hedgehog. *J Physiol*. 1942. doi:10.1113/jphysiol.1942.sp003955
3. Bressler SL, Freeman WJ. Frequency analysis of olfactory system EEG in cat, rabbit, and rat. *Electroencephalogr Clin Neurophysiol*. 1980. doi:10.1016/0013-4694(80)90319-3
4. Laurent G, Naraghi M. Odorant-induced oscillations in the mushroom bodies of the locust. *J Neurosci*. 1994. doi:10.1523/jneurosci.14-05-02993.1994
5. Gelperin A. Nitric oxide mediates network oscillations of olfactory interneurons in a terrestrial mollusc. *Nature*. 1994. doi:10.1038/369061a0
6. Kay LM. Olfactory system oscillations across phyla. *Curr Opin Neurobiol*. 2015. doi:10.1016/j.conb.2014.10.004
7. Eeckman FH, Freeman WJ. Correlations between unit firing and EEG in the rat olfactory system. *Brain Res*. 1990. doi:10.1016/0006-8993(90)91663-2
8. Mazo C, Lepousez G, Nissant A, Valley MT, Lledo PM. GABAb receptors tune cortical feedback to the olfactory bulb. *J Neurosci*. 2016. doi:10.1523/JNEUROSCI.3823-15.2016
9. Kay LM, Beshel J, Brea J, Martin C, Rojas-Líbano D, Kopell N. Olfactory oscillations: the what, how and what for. *Trends Neurosci*. 2009. doi:10.1016/j.tins.2008.11.008
10. Gelperin A. Olfactory computations and network oscillations. *J Neurosci*. 2006. doi:10.1523/JNEUROSCI.3737-05b.2006
11. Martin C, Ravel N. Beta and gamma oscillatory activities associated with olfactory memory tasks: Different rhythms for different functional networks? *Front Behav Neurosci*. 2014. doi:10.3389/fnbeh.2014.00218
12. Jessberger J, Zhong W, Brankačk J, Draguhn A. Olfactory Bulb Field Potentials and Respiration in Sleep-Wake States of Mice. *Neural Plast*. 2016. doi:10.1155/2016/4570831
13. Cox JPL. Hydrodynamic aspects of fish olfaction. *J R Soc Interface*. 2008. doi:10.1098/rsif.2007.1281
14. Nevitt GA. Do fish sniff? A new mechanism of olfactory sampling in pleuronectid flounders. *J Exp Biol*. 1991. doi:10.1242/jeb.157.1.1
15. Kay LM. Circuit oscillations in odor perception and memory. In: *Progress in Brain Research*. ; 2014. doi:10.1016/B978-0-444-63350-7.00009-7
16. Jia X, Kohn A. Gamma rhythms in the brain. *PLoS Biol*. 2011. doi:10.1371/journal.pbio.1001045
17. Kay LM, Stopfer M. Information processing in the olfactory systems of insects and vertebrates. *Semin Cell Dev Biol*. 2006. doi:10.1016/j.semcdb.2006.04.012
18. Wilson RI, Mainen ZF. Early events in olfactory processing. *Annu Rev Neurosci*. 2006. doi:10.1146/annurev.neuro.29.051605.112950
19. Tabor R, Yaksi E, Friedrich RW. Multiple functions of GABAA and GABAB receptors during pattern processing in the zebrafish olfactory bulb. *Eur J Neurosci*. 2008. doi:10.1111/j.1460-9568.2008.06316.x
20. Laurent G. Olfactory network dynamics and the coding of multidimensional signals. *Nat Rev Neurosci*. 2002. doi:10.1038/nrn964
21. Poo C, Isaacson JS. Odor Representations in Olfactory Cortex: “Sparse” Coding, Global Inhibition, and Oscillations. *Neuron*. 2009. doi:10.1016/j.neuron.2009.05.022
22. Frederick DE, Brown A, Brim E, Mehta N, Vujovic M, Kay LM. Gamma and beta oscillations define a sequence of neurocognitive modes present in odor processing. *J Neurosci*. 2016. doi:10.1523/JNEUROSCI.0569-16.2016
23. Olivares J, Schmachtenberg O. An update on anatomy and function of the teleost olfactory system. *PeerJ*. 2019. doi:10.7717/peerj.7808
24. Butler AB, Hodos W. *Comparative Vertebrate Neuroanatomy: Evolution and Adaptation: Second*

Edition.; 2005. doi:10.1002/0471733849
25. Ferrando S, Gallus L, Gambardella C, et al. Neuronal nitric oxide synthase (nNOS) immunoreactivity in the olfactory system of a cartilaginous fish. *J Chem Neuroanat*. 2012. doi:10.1016/j.jchemneu.2012.03.005
26. Nikonov AA, Caprio J. Odorant specificity of single olfactory bulb neurons to amino acids in the channel catfish. *J Neurophysiol*. 2004. doi:10.1152/jn.00023.2004
27. Nieuwenhuys R, ten Donkelaar HJ, Nicholson C. *The Central Nervous System of Vertebrates*.; 1998. doi:10.1007/978-3-642-18262-4
28. Portavella M, Vargas JP. Emotional and spatial learning in goldfish is dependent on different telencephalic pallial systems. *Eur J Neurosci*. 2005. doi:10.1111/j.1460-9568.2005.04114.x
29. Ito H, Yamamoto N. Non-laminar cerebral cortex in teleost fishes? *Biol Lett*. 2009. doi:10.1098/rsbl.2008.0397
30. Biechl D, Tietje K, Ryu S, Grothe B, Gerlach G, Wullimann MF. Identification of accessory olfactory system and medial amygdala in the zebrafish. *Sci Rep*. 2017. doi:10.1038/srep44295
31. Broglio C, Rodríguez F, Salas C. Spatial cognition and its neural basis in teleost fishes. *Fish Fish*. 2003. doi:10.1046/j.1467-2979.2003.00128.x
32. Cerdá-Reverter JM, Zanuy S, Muñoz-Cueto JA. A Cytoarchitectonic study of the brain of a perciform species, the sea bass (Dicentrarchus labrax). I. The telencephalon. *J Morphol*. 2001. doi:10.1002/1097-4687(200103)247:3<217::AID-JMOR1013>3.0.CO;2-U
33. Folgueira M, Anadón R, Yáñez J. An experimental study of the connections of the telencephalon in the rainbow trout (Oncorhynchus mykiss). I: Olfactory bulb and ventral area. *J Comp Neurol*. 2004. doi:10.1002/cne.20340
34. Kermen F, Franco LM, Wyatt C, Yaksi E. Neural circuits mediating olfactory-driven behavior in fish. *Front Neural Circuits*. 2013. doi:10.3389/fncir.2013.00062
35. Mueller T, Dong Z, Berberoglu MA, Guo S. The dorsal pallium in zebrafish, Danio rerio (Cyprinidae, Teleostei). *Brain Res*. 2011. doi:10.1016/j.brainres.2010.12.089
36. Wullimann MF, Rink E. The teleostean forebrain: A comparative and developmental view based on early proliferation, Pax6 activity and catecholaminergic organization. In: *Brain Research Bulletin*. ; 2002. doi:10.1016/S0361-9230(01)00666-9
37. Rolen SH, Caprio J. Bile salts are effective taste stimuli in channel catfish. *J Exp Biol*. 2008. doi:10.1242/jeb.018648
38. Calfún C, Domínguez C, Pérez-Acle T, Whitlock KE. Changes in olfactory receptor expression are correlated with odor exposure during early development in the zebrafish (Danio rerio). *Chem Senses*. 2016. doi:10.1093/chemse/bjw002
39. Mathuru AS, Kibat C, Cheong WF, et al. Chondroitin fragments are odorants that trigger fear behavior in fish. *Curr Biol*. 2012. doi:10.1016/j.cub.2012.01.061
40. Valdés J, Olivares J, Ponce D, Schmachtenberg O. Analysis of olfactory sensitivity in rainbow trout (Oncorhynchus mykiss) reveals their ability to detect lactic acid, pyruvic acid and four B vitamins. *Fish Physiol Biochem*. 2015. doi:10.1007/s10695-015-0054-9
41. Wisenden BD, Rugg ML, Korpi NL, Fuselier LC. Lab and field estimates of active time of chemical alarm cues of a cyprinid fish and an amphipod crustacean. *Behaviour*. 2009. doi:10.1163/156853909X440998
42. Olivares J. PhD Thesis. *Univ Valparaiso, Chile*.
43. Fahrenfort JJ, van Driel J, van Gaal S, Olivers CNL. From ERPs to MVPA using the Amsterdam Decoding and Modeling toolbox (ADAM). *Front Neurosci*. 2018;12(JUL). doi:10.3389/fnins.2018.00368
44. Hebart MN, Baker CI. Deconstructing multivariate decoding for the study of brain function. *Neuroimage*. 2018;180:4-18. doi:10.1016/j.neuroimage.2017.08.005
45. Maris E, Oostenveld R. Nonparametric statistical testing of EEG- and MEG-data. *J Neurosci Methods*. 2007;164(1):177-190. doi:10.1016/j.jneumeth.2007.03.024
46. Le Van Quyen M, Foucher J, Lachaux J, et al. Comparison of Hilbert transform and wavelet methods for the analysis of neuronal synchrony. *J Neurosci Methods*. 2001;111(2):83-98.

http://www.ncbi.nlm.nih.gov/pubmed/11595276.
47. Fries P. A mechanism for cognitive dynamics: Neuronal communication through neuronal coherence. *Trends Cogn Sci*. 2005;9(10):474-480. doi:10.1016/j.tics.2005.08.011
48. Imperatori LS, Betta M, Cecchetti L, et al. EEG functional connectivity metrics wPLI and wSMI account for distinct types of brain functional interactions. *Sci Rep*. 2019;9(1). doi:10.1038/s41598-019-45289-7
49. Stam CJ, Nolte G, Daffertshofer A. Phase lag index: Assessment of functional connectivity from multi channel EEG and MEG with diminished bias from common sources. *Hum Brain Mapp*. 2007;28(11):1178-1193. doi:10.1002/hbm.20346
50. Vinck M, Oostenveld R, Van Wingerden M, Battaglia F, Pennartz CMA. An improved index of phase-synchronization for electrophysiological data in the presence of volume-conduction, noise and sample-size bias. *Neuroimage*. 2011;55(4):1548-1565. doi:10.1016/j.neuroimage.2011.01.055
51. King JR, Sitt JD, Faugeras F, et al. Information sharing in the brain indexes consciousness in noncommunicative patients. *Curr Biol*. 2013;23(19):1914-1919. doi:10.1016/j.cub.2013.07.075
52. Canales-Johnson A, Billig AJ, Olivares F, et al. Dissociable Neural Information Dynamics of Perceptual Integration and Differentiation during Bistable Perception. *Cereb Cortex*. 2020. doi:10.1093/cercor/bhaa058
53. Sitt JD, King JR, El Karoui I, et al. Large scale screening of neural signatures of consciousness in patients in a vegetative or minimally conscious state. *Brain*. 2014;137(8):2258-2270. doi:10.1093/brain/awu141
54. Ince RAA. Measuring multivariate redundant information with pointwise common change in surprisal. *Entropy*. 2017;19(7). doi:10.3390/e19070318
55. Ince RAA, Giordano BL, Kayser C, Rousselet GA, Gross J, Schyns PG. A statistical framework for neuroimaging data analysis based on mutual information estimated via a gaussian copula. *Hum Brain Mapp*. 2017. doi:10.1002/hbm.23471
56. Salazar RF, Dotson NM, Bressler SL, et al. Content-specific fronto-parietal synchronization during visual working memory. *Science*. 2012;338(6110):1097-1100. doi:10.1126/science.1224000
57. Saalmann YB, Pinsk MA, Wang L, Li X, Kastner S. The pulvinar regulates information transmission between cortical areas based on attention demands. *Science (80-)*. 2012. doi:10.1126/science.1223082
58. Bastos AM, Schoffelen JM. A tutorial review of functional connectivity analysis methods and their interpretational pitfalls. *Front Syst Neurosci*. 2016. doi:10.3389/fnsys.2015.00175
59. Canales-Johnson A, Beerendonk L, Blain S, et al. Decreased alertness reconfigures cognitive control networks. *J Neurosci*. 2020. doi:10.1523/JNEUROSCI.0343-20.2020
60. Rabinovich MI, Huerta R, Volkovskii A, Abarbanel HDI, Stopfer M, Laurent G. Dynamical coding of sensory information with competitive networks. In: *Journal of Physiology Paris*. ; 2000. doi:10.1016/S0928-4257(00)01092-5
61. Ince RAA, Giordano BL, Kayser C, Rousselet GA, Gross J, Schyns PG. A statistical framework for neuroimaging data analysis based on mutual information estimated via a gaussian copula. *Hum Brain Mapp*. 2017;38(3):1541-1573. doi:10.1002/hbm.23471
62. Freeman WJ, Schneider W. Changes in Spatial Patterns of Rabbit Olfactory EEG with Conditioning to Odors. *Psychophysiology*. 1982. doi:10.1111/j.1469-8986.1982.tb02598.x
63. Kay LM, Laurent G. Odor- and context-dependent modulation of mitral cell activity in behaving rats. *Nat Neurosci*. 1999. doi:10.1038/14801
64. Miller KJ, Sorensen LB, Ojemann JG, Den Nijs M. Power-law scaling in the brain surface electric potential. *PLoS Comput Biol*. 2009;5(12). doi:10.1371/journal.pcbi.1000609
65. Canales-Johnson A, Borges AFT, Komatsu M, et al. Broadband Dynamics Rather than Frequency-Specific Rhythms Underlie Prediction Error in the Primate Auditory Cortex. *J Neurosci*. 2021;41(45):9374-9391.
66. Freeman WJ, Zhai J. Simulated power spectral density (PSD) of background electrocorticogram (ECoG). *Cogn Neurodyn*. 2009;3(1):97-103. doi:10.1007/s11571-008-9064-y
67. Buzsáki G, Anastassiou C a, Koch C. The origin of extracellular fields and currents--EEG, ECoG, LFP and spikes. *Nat Rev Neurosci*. 2012;13(6):407-420. doi:10.1038/nrn3241
68. Donoghue T, Schaworonkow N, Voytek B. Methodological considerations for studying neural

oscillations. *Eur J Neurosci*. 2021. doi:10.1111/ejn.15361
69. Yaksi E, Von Saint Paul F, Niessing J, Bundschuh ST, Friedrich RW. Transformation of odor representations in target areas of the olfactory bulb. *Nat Neurosci*. 2009. doi:10.1038/nn.2288
70. Marder E. Variability, compensation, and modulation in neurons and circuits. *Proc Natl Acad Sci U S A*. 2011. doi:10.1073/pnas.1010674108
71. Whitacre J, Bender A. Degeneracy: A design principle for achieving robustness and evolvability. *J Theor Biol*. 2010. doi:10.1016/j.jtbi.2009.11.008
72. Edelman GM, Gally JA. Degeneracy and complexity in biological systems. *Proc Natl Acad Sci U S A*. 2001. doi:10.1073/pnas.231499798
73. Tononi G, Sporns O, Edelman GM. Measures of degeneracy and redundancy in biological networks. *Proc Natl Acad Sci U S A*. 1999. doi:10.1073/pnas.96.6.3257
74. Driscoll LN, Pettit NL, Minderer M, Chettih SN, Harvey CD. Dynamic Reorganization of Neuronal Activity Patterns in Parietal Cortex. *Cell*. 2017. doi:10.1016/j.cell.2017.07.021
75. Druckmann S, Chklovskii DB. Neuronal circuits underlying persistent representations despite time varying activity. *Curr Biol*. 2012. doi:10.1016/j.cub.2012.08.058
76. Murray JD, Bernacchia A, Roy NA, Constantinidis C, Romo R, Wang XJ. Stable population coding for working memory coexists with heterogeneous neural dynamics in prefrontal cortex. *Proc Natl Acad Sci U S A*. 2017. doi:10.1073/pnas.1619449114
77. Moreno-Bote R, Beck J, Kanitscheider I, Pitkow X, Latham P, Pouget A. Information-limiting correlations. *Nat Neurosci*. 2014. doi:10.1038/nn.3807